# COMPUTATIONAL FLUID DYNAMICS SIMULATION OF AIRFLOW THROUGH STANDING VEGETATION

H. B. Gonzales, J. Tatarko, M. E. Casada, R. G. Maghirang,
L. J. Hagen, C. J. Barden

## HIGHLIGHTS

- Measured airflow through a simulated canopy was successfully modeled using CFD software.
- Effective drag coefficients did not differ between the experimental and simulated results.
- Results of this study provide 3-D simulation data of wind flow through a plant canopy.

**ABSTRACT.** *Maintaining vegetative cover on the soil surface is the most widely used method for control of soil loss by wind erosion. We numerically modeled airflow through artificial standing vegetation (i.e., simulated wheat plants) using computational fluid dynamics (CFD). A solver (simpleFoam within the OpenFOAM software architecture) was used to simulate airflow through various three-dimensional (3D) canopy structures in a wind tunnel, which were created using another open-source CAD geometry software (Salomé ver. 7.2). This study focused on two specific objectives: (1) model airflow through standing vegetation using CFD, and (2) compare the results of a previous wind tunnel study with various artificial vegetation configurations to the results of the CFD model. Wind speeds measured in the wind tunnel experiment differed slightly from the numerical simulation using CFD, especially near positions where simulated vegetation was present. Effective drag coefficients computed using wind profiles did not differ significantly ($p < 0.05$) between the experimental and simulated results. Results of this study will provide information for research into other types of simulated stubble or sparse vegetation during wind erosion events.*

***Keywords.*** *3-D canopy structure, OpenFOAM, Wind erosion, Wind tunnel studies.*

Wind erosion poses a significant risk to agricultural lands despite numerous mitigation strategies employed for its control. One such control strategy is the maintenance of vegetation cover. When vegetation is sparse, standing residue is significantly more effective than flat residue for wind erosion control (Hagen, 1996). Wind erosion studies have focused on the effects of sparse vegetation after harvesting (Wolfe and Nickling, 1993; Lancaster and Baas, 1998; He et al., 2017), land degradation and conversion (Li et al., 2005), and dry land conditions (Musick and Gillette, 1990; Toure et al., 2011). These are all conditions that make the soil surface vulnerable to wind erosion.

Previous studies have used wind tunnels to identify parameters and processes that influence wind erosion. Lyles and Allison (1976) compared spacings and orientations of standing stubble for mitigating wind erosion. Their study showed that a stubble row orientation perpendicular to the wind was more effective than a parallel orientation for sheltering against wind erosion. Densities of simulated plant stalks with various diameters and heights were employed by van de Ven et al. (1989), who reported up to 82% reduction in soil loss due to the presence of stalks. Hagen and Armbrust (1994) proposed a theoretical approach, including surface friction velocity reduction and interception of saltation in standing stalks, to predict the amount of soil loss. They found a correlation ($R^2 = 0.89$) between soil loss reduction and the plant area index of stalks. Standing sticks were used in a wind tunnel study by Dong et al. (2001) to demonstrate that the height and density of standing vegetation influence the roughness length and drag coefficient. They also deduced that the height/spacing ratio is the most essential structural parameter that influences drag coefficients and roughness lengths. In wind tunnel studies of simulated broadleaf (e.g., soybean) canopies with varying leaf distribution by height, Hagen and Casada (2013) found that can-

Submitted for review in April 2019 as manuscript number NRES 13449; approved for publication as a Research Article by the Natural Resources & Environmental Systems Community of ASABE in October 2019.

Mention of company or trade names is for description only and does not imply endorsement by the USDA. The USDA is an equal opportunity provider and employer.

The authors are **Howell B. Gonzales,** Former Graduate Research Assistant, Department of Biological and Agricultural Engineering, Kansas State University, Manhattan, Kansas; **John Tatarko,** Soil Scientist, USDA-ARS Rangeland Resources and Systems Research Unit, Fort Collins, Colorado; **Mark E. Casada,** Research Agricultural Engineer, USDA-ARS Stored Product Insect and Engineering Research Unit, Manhattan, Kansas; **Ronaldo G. Maghirang,** Professor, Department of Biological and Agricultural Engineering, Kansas State University, Manhattan, Kansas; **Lawrence J. Hagen,** Research Agricultural Engineer (Retired), USDA-ARS Stored Product Insect and Engineering Research Unit, Manhattan, Kansas; **Charles J. Barden,** Professor, Department of Horticulture and Natural Resources, Kansas State University, Manhattan, Kansas. **Corresponding author:** John Tatarko, USDA-ARS RRSRU, 2150 Centre Avenue, Bldg. D, Suite 200, Fort Collins, CO 80526; phone: 970-492-7320; e-mail: john.tatarko@usda.gov.

opy leaf area index (LAI) was directly related to threshold velocity and inversely related to sand transport capacity. The canopies modified both the wind profile and the normalized abrasion energy of the sand discharge when compared with a bare sandy surface. Vegetation density was also found by Gonzales et al. (2017) to be directly related to threshold velocity and inversely related to sand discharge. The presence of vegetation was found to be effective in minimizing abrasion of standing vegetation models by lowering the saltation of sand particles that could impact the simulated plants.

Field studies have also been conducted to determine the effects of vegetated surfaces on wind erosion. Stockton and Gillette (1990) evaluated three test sites. They found that dense vegetation resulted in large sheltered areas, as evidenced by the small ratios of threshold friction velocities for a vegetated surface over a bare soil surface. Their measurements showed that the ratios ranged from 0.27 to 0.44, in which a value of 1.0 denotes a bare sand configuration. Li et al. (2005) conducted a study in China which showed that early stages of vegetation were more prone to wind erosion on degraded grasslands, while established grasses showed greater resistance to wind erosion. They found that the wind erosion reduction on fixed (vegetated) land was 1/47 (2.13%) of that on shifting (loose and bare) sandy land.

Field measurements should ensure realistic surface conditions (Fryrear et al., 1991), whereas with wind tunnels, it is necessary to control the meteorological and surface parameters (e.g., wind speed, soil type, vegetation element type, and vegetation configuration). Both field and wind tunnel testing are expensive and time-consuming. Numerical simulation, such as computational fluid dynamics (CFD), combined with sufficient validation, has provided an alternative approach in a wide range of research (Politis et al., 2008; Qiao and Liu, 2008; Defraeye et al., 2010; Bonifacio et al., 2014).

Numerical simulation of various types of vegetation (natural and artificial) using commercially available CFD software (e.g., Fluent) has been studied extensively. Tiwary et al. (2005) used the shear stress transport turbulence model described by Menter (1994) to simulate airflow across three hedge species (hawthorn, holly, and yew). Lin et al. (2007) employed the shear stress transport $k$-ω model to study airflow and odor dispersion across tree shelterbelts. Investigating airflow through various configurations of cypress trees, Rosenfeld et al. (2010) used individual trees as well as multiple rows to compare to their experimental results. They concluded that reduction in airflow and lateral variations in wind speed were caused by canopy density. Gromke et al. (2008) investigated airflow and exhaust dispersion across trees planted along roads in an urban street canyon. They found that the Reynolds stress model was better than the standard $k$-ε turbulence model for predicting dispersion occurring within trees. On the other hand, Endalew et al. (2009) attempted to model the 3D architecture of leafless plant canopies using commercial CFD software. They employed the standard $k$-ε turbulence model and found that predicted velocities agreed with experimental results. Bitog et al. (2012) compared wind tunnel measurements of airflow across black pine trees to CFD simulations. They used the re-normalization group (RNG) $k$-ε turbulence model and assessed the effects of gaps and rows between trees. Guo and Maghirang (2012) compared the experimental values of Tiwary et al. (2005) to CFD simulations using the standard $k$-ε and realizable $k$-ε turbulence closure models; they found good agreement between the two models.

Open-source CFD software, such as OpenFOAM, has gained popularity in many disciplines because of the high cost of commercial CFD packages. Lysenko et al. (2013) reported that the performances of FLUENT and OpenFOAM were comparable in simulating flows across a bluff body. Higuera et al. (2013) used OpenFOAM to validate a newly developed wave generation and active absorption boundary condition. They found that water waves were generated realistically, and the agreement between laboratory and numerical data was very high regarding wave breaking, run up, and undertow currents. Bonifacio et al. (2014) compared the results of AERMOD and OpenFOAM in simulating particle transport from a ground-level source. They found that the two models responded similarly to effects of atmospheric stability and wind speed.

Most CFD studies of wind flow through vegetation have been made on windbreaks, with few, if any, conducted within crop plant canopies. In this study, we used CFD to numerically model the airflow through artificial standing vegetation (i.e., simulated wheat plants) that were previously measured by Gonzales et al. (2017). A specific solver of the OpenFOAM architecture (simpleFoam) was used to simulate airflow through a 3D canopy structure in the wind tunnel. A numerical representation of the 3D canopy was created using another open-source CAD geometry software (Salomé ver. 7.2) to address the following objectives:

1. Model airflow through multiple standing vegetation canopy configurations using open-source CFD software.
2. Compare the results of a previous wind tunnel study with various artificial vegetation configurations to the results of the CFD model.

## MATERIALS AND METHODS

### WIND TUNNEL EXPERIMENT

A detailed description of the wind tunnel experiment that was the basis for comparison with the CFD simulation is provided by Gonzales et al. (2017). Briefly, in that study, a series of wind tunnel experiments was conducted to measure airflow using a rack of pitot tubes within simulated standing wheat vegetation (i.e., split plastic straws). Wind speed profiles were evaluated during 3 min test runs at two different vegetation heights (150 and 220 mm) for each of three densities of the simulated vegetation (i.e., 100 mm × 200 mm, 200 mm × 200 mm, and 300 mm × 200 mm spacing). The wind speed ($U_{max}$) was a constant 15 m $s^{-1}$.

Comparisons were based on wind velocity measurements from the pitot tube system within the artificial standing vegetation. An array of eleven pitot-static tubes was deployed at two heights, giving velocity measurements at 22 total heights up to 0.5 m above the surface. An additional pitot tube measured the free-stream velocity at 0.9 m above the

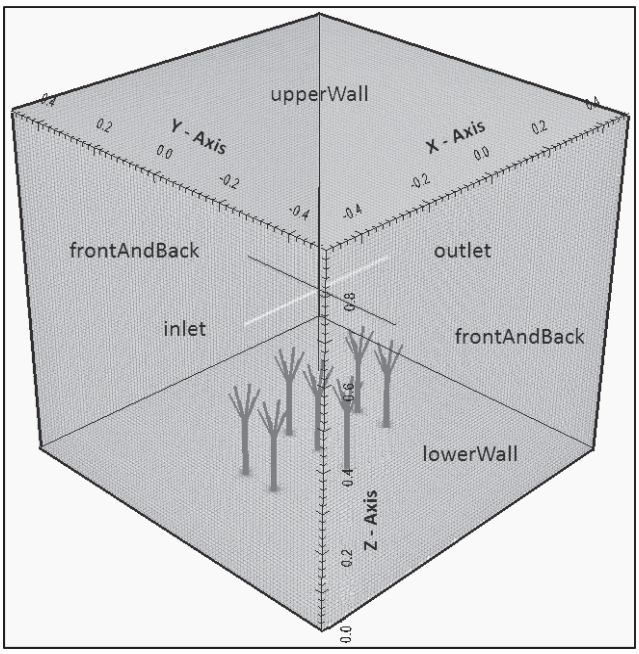


**Figure 1. Computational domain for airflow through artificial standing vegetation using ParaView visualization within OpenFOAM.**

surface. There were three replications of each test. The pitot tube measurements within the height of the canopy were analyzed for canopy effects. Velocity profiles from the experiment were used to determine effective drag coefficient ($C_n$) values within the standing vegetation and were compared to the results of CFD simulation. A detailed derivation of the equation for $C_n$ was shown by Endalew et al. (2009). The resulting final equation used in this study is:

$$C_n(z) = \frac{1}{LA} \ln \frac{U_{up}(z)}{U_{down}(z)} \quad (1)$$

where $C_n(z)$ is the value of $C_n$ at various vertical positions, $L$ is the distance between upwind and downwind positions of wind velocity measurements (m), $A$ is the leaf area density ($m^{-1}$), which is defined here as the leaf area per unit volume, $U_{up}(z)$ is the mean vertical velocity in the upwind position, and $U_{down}(z)$ is the mean vertical velocity in the downwind position. Mean values for upwind and downwind locations include velocity measurements taken along a single line at the back or front of the canopy. For example, at a constant value of $x$ ($x$ = position downwind), velocities must be taken at a range of $y$-values ($y$ = position across the tunnel) upwind and at the same range of $y$-values downwind along the vertical height ($z$) of the canopy, as shown in figure 1. Mean values of velocity were also used for comparing the overall canopy velocity profiles from the experiments to those from the simulations.

## COMPUTATIONAL DOMAIN

The computational domain (fig. 1 and table 1) is based on measurements by Gonzales et al. (2017) of wind velocity profiles in a wind tunnel where the maximum height of the domain corresponds to the free-stream velocity measured in the wind tunnel (i.e., free-stream velocity was measured at 0.9 m above the tunnel floor). The length and width of the domain were limited by the number of standing artificial vegetation elements chosen to represent the simulation to minimize computation time while representing changes between wind profiles. For this study, seven elements (i.e., individual plants; fig. 1) were used to compute wind velocities between rows for three artificial vegetation configurations within the tunnel (100 mm × 200 mm, 200 mm × 200 mm, and 300 mm × 200 mm spacings) and two vegetation heights (150 and 220 mm).

**Table 1. Computational grid for artificial standing vegetation.**

| | | |
|---|---|---|
| Number of cells | | 1,046,096 |
| Number of faces | | 3,258,462 |
| Number of nodes | | 1,172,843 |
| $x$-Coordinate | Minimum | -0.5 m |
| | Maximum | 0.5 m |
| $y$-Coordinate | Minimum | -0.5 m |
| | Maximum | 0.5 m |
| $z$-Coordinate | Minimum | 0.0 m |
| | Maximum | 0.9 m |

## NUMERICAL SIMULATION

During the preprocessing phase of the CFD modeling, the geometry and domain for the mesh were created. This study used external flow, and the geometry and domain were created accordingly. OpenFOAM (ver. 2.2.2, OpenCFD, Bracknell, UK; https://openfoam.org) was the CFD software used in this study. Processing requires a specific solver within the OpenFOAM solution binaries, which are programmed using C++. Post-processing was performed using the included ParaView application that automatically visualizes the simulation solution. Values generated from the solution were also exported and visualized within a spreadsheet for cross-checking and validation.

### *Governing Equations*

This study focused on turbulent airflow through a canopy (i.e., artificial standing vegetation). The Reynolds-averaged Navier-Stokes (RANS) method was adopted because it is able to represent the turbulent components of instantaneous velocities of the fluid. Equations were based on 3D RANS steady-state, incompressible, and isothermal conditions, taking the turbulent atmospheric layer as neutrally stratified (Guo and Maghirang, 2012), with mass transfer neglected. Continuity and momentum conservation equations are presented in detail by Cheng et al. (2003), Endalew et al. (2009), and Yeh et al. (2010). The complete formulation of the RNG $k$-ε turbulence model used in this study was presented by Yeh et al. (2010). Previous studies indicated that the RNG $k$-ε model was the most suitable turbulence model for investigating complex wind flows around barriers (Packwood, 2000; Lee and Lim, 2001; Lee et al., 2007; Li et al., 2007; Santiago et al., 2007; Bourdin and Wilson, 2008; Yeh et al., 2010; Bitog et al., 2012). The input parameters of the turbulence model are defined in table 2.

### *Geometry and Mesh Generation*

For OpenFOAM, geometries for internal flows are typically created using a meshing tool, known as blockMesh, which creates fully structured hexahedral meshes. For external flow, as in this study, blockMesh cannot be used. For this

**Table 2. Input parameter values used for CFD simulation of airflow through artificial standing vegetation (based on OpenCFD, 2011; Guo and Maghirang, 2012; Bonifacio et al., 2014).**

| Parameter | Symbol | Value |
|---|---|---|
| Air density (kg m$^{-3}$) | $\rho$ | 1.225 |
| Air dynamic viscosity (kg m$^{-1}$ s$^{-1}$) | $\mu$ | $1.79 \times 10^{-5}$ |
| Kinematic viscosity (m$^2$ s$^{-1}$) | $\upsilon$ | $1.46 \times 10^{-5}$ |
| Turbulence model constant | $C_{1\varepsilon}$ | 1.42 |
| Turbulence model constant | $C_{2\varepsilon}$ | 1.68 |
| Turbulence model constant | $C_\mu$ | 0.085 |
| Turbulence model constant | $\beta$ | 0.012 |
| Turbulence model constant | $\eta_o$ | 4.38 |
| Turbulent Prandtl number for $k$ | $\sigma_k$ | 0.719 |
| Turbulent Prandtl number for $\varepsilon$ | $\sigma_\varepsilon$ | 0.719 |
| von Karman constant | $\kappa$ | 0.4187 |

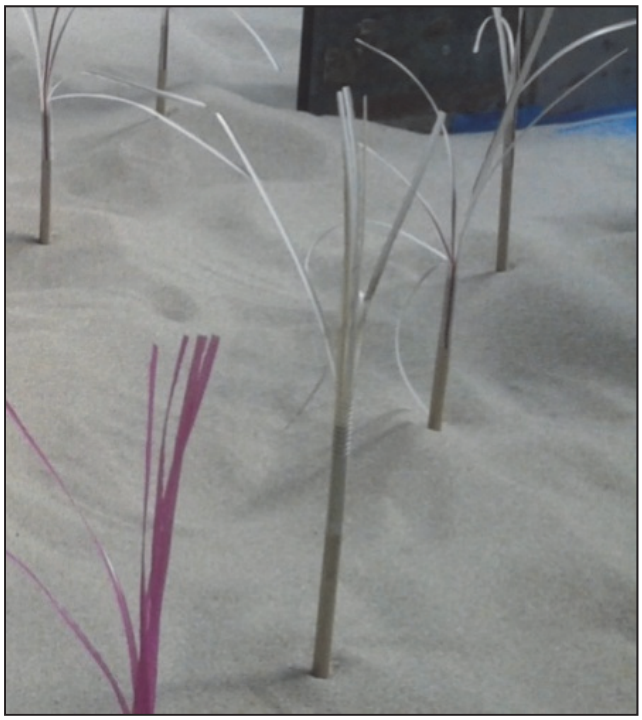

**Figure 2. Artificial standing vegetation model of wheat that was used in the wind tunnel study.**

study, 3D geometry was based on the artificial standing vegetation used in the wind tunnel (fig. 2). Third-party software (Salomé ver. 7.2, Open Cascade, Guyancourt, France; http://www.salome-platform.org) was used to create the geometry to be "snapped" or overlapped with the block domain using the other mesh tool of OpenFOAM, known as snappyHexMesh, a built-in meshing tool for creating internal faces within a domain to evaluate external flows. The created 3D models were exported as a stereolithography (.stl) file in ASCII format (the format recognized by snappyHexMesh).

## CFD Solution Method

SimpleFoam, which is a solver applicable to steady-state, incompressible turbulent flow, was used for this study. It uses the semi-implicit method for the pressure-linked equation (SIMPLE) algorithm developed by Patankar (1980) for decoupling pressure and velocity (OpenCFD, 2011). For a specific solver, various types of files are necessary.

### *Boundary Conditions*

Boundaries for the entire domain were set up in the format read by SimpleFoam. Initial values for $\varepsilon$, $k$, pressure ($p$), and air velocity ($U$) were used in the solver and were placed as separate files to be read by the solver. These values were set for boundary regions in the domain, namely, the inlet, outlet, upperWall, lowerWall, and frontAndBack regions (fig. 1). Inlet values for $\varepsilon$ and $k$ were based on the equilibrium boundary layer assumption described by Richards and Hoxey (1993), Santiago et al. (2007), Bourdin and Wilson (2008), Yeh et al. (2010), and Guo and Maghirang (2012) and were obtained by the following equations:

$$k_{in} = \frac{u_*^2}{\sqrt{C_\mu}} \tag{2}$$

$$\varepsilon_{in} = \frac{u_*^3}{\kappa z} \tag{3}$$

where $u_*$ is the friction velocity far upstream of the vegetation (from the wind tunnel tests, $u_* = 0.24$ m s$^{-1}$), $C_\mu$ is the turbulence model constant, $\kappa$ is the von Karman constant (both provided in table 2), and $z$ is the height above the tunnel floor (m). Pressure was initially set as zero (0 Pa) inside the domain (internalField in OpenFOAM). Pressure was also given a zero gradient for the inlet, upperWall, and frontAndBack, with a symmetry condition for upperWall, and a constant outlet value. For other regions in the domain, outlet flow was given a fully developed flow condition (i.e., zero velocity gradient), symmetry conditions at the upperWall and frontAndBack regions, no-slip condition at the lowerWall, and near-wall conditions for $\varepsilon$ and $k$ (i.e., *epsilonWallFunction* and *kqrWallFunction*, respectively) for all other domain regions used (Liu, 2016).

Initial values inside the domain (internalField in OpenFOAM) for all parameters were set to zero. Wind velocity measurements during the wind tunnel experiment served as input values for $x$-component inlet velocities ($u_x$); other velocity components ($u_y$ and $u_z$) were assumed to be zero.

### *Post-Processing*

Visualization of simulation results was done in the OpenFOAM application ParaView 3.40. During computation (iteration steps), OpenFOAM interim results were cross-checked for stability, unboundedness, and residual behavior by installing GNUPlot to visualize the results to ensure that the parameters computed during the numerical simulation were acceptable, whether or not convergence was met.

Velocity profiles measured during the wind tunnel experiment with various standing vegetation configurations were compared to the simulation results. A useful option in ParaView was to filter out desired points or regions within the domain to export data from within ParaView. Failure to do so can lead to an error when the entire set of data exceeds the maximum allowable rows in the spreadsheet program, which is common if the mesh contains millions of cells.

### *Data Analysis*

Mean values of predicted and experimental wind velocities and drag coefficients were compared using the normality

and homogeneity of variances assumption and a standard statistical paired t-test in Excel (Microsoft Corp., Redmond, Wash.). An analysis of variance (ANOVA) was performed to determine the effect of vegetation densities and heights. A 5% level of significance was used for all cases. CurveExpert 1.4 (Hyams, 2013) was used to plot best-fit curves.

## Results and Discussion

### Geometry and Mesh Generation

Figure 3a shows the 3D model for the artificial standing vegetation created using Salomé. The ".stl" file format of the 3D geometry was called within the dictionary of the snappyHexMesh meshing tool of OpenFOAM. In addition to geometry reconstruction, much mesh parameter conditioning (i.e., level refinement, layer refinement, angles) was needed and evaluated by trial-and-error to obtain an acceptable mesh (fig. 3b) to proceed with the iteration steps of the simulation (i.e., a very fine mesh led to a very long computational procedure). Although mesh quality increased with the addition of sublayers, especially at the edges of the geometries in the snappyHexMesh step, the decision was made to ignore adding sublayers because the geometry was too small to add more layers, and the mesh created almost always failed in the mesh checks when sublayers were added. During mesh creation, the mesh size of the domain (through blockMesh) dictates whether or not problematic faces are created because, by default, snappyHexMesh creates a very fine mesh. Therefore, if blockMesh has a coarse mesh and the "snapped" figure has a relatively fine mesh, failed mesh checks would result in unboundedness and divergence of the solution.

### Comparison of CFD Results with Experimental Results

Figure 4 shows values of $C_n$ for the various standing vegetation configurations, where the vertical height ($z$) was normalized with the height of the canopy. The drag coefficients are low at the bottom of the canopy and return to zero above the canopy. With no obstructions, drag coefficients are always zero. Numerical values of $C_n$ did not differ significantly ($p < 0.05$) between the CFD simulation and experimental results; however, the profile shapes were slightly different, especially for denser configurations (100 mm × 200 mm), possibly a result of pertinent oscillations of the airflow that created excessive turbulence as the density of standing vegetation increased. Slight discrepancies in the profile shape can be caused by oscillations (bending motions) in the upper portion of the standing vegetation as air travels through it. These oscillations of the standing vegetation were not simulated during CFD simulation.

A comparison of the normalized wind profiles is shown in figure 5 for the densest vegetation configuration of 100 mm × 200 mm at 220 mm height, which is illustrated in figure 6. The comparison was made at velocities measured at 100 mm from the back of the canopy. This measurement is essentially half of the constant row spacing (200 mm) of the configuration. Vertical height ($z$) was normalized with the height of the canopy, while wind velocity ($U$) was normalized by the maximum velocity for the simulation or experiment. The maximum velocity in the OpenFOAM simulation occurred at the top boundary of the domain ($z$ = 0.9 m), which was the height of free-stream velocity during the wind tunnel experiment, coinciding with the maximum velocity in the tunnel.

Differences in the velocity profiles between the wind tunnel values and CFD simulation results are evident in figure 5. The simulation results show dramatic decreases in velocity at the crown of the canopy, where the split in the straws occurred. However, the measured values did not exhibit such a dramatic, isolated decrease. The measurements showed a limited decrease in velocity (limited change in profile shape) at the wake of the canopy, but fluctuating values of wind velocity were evident. This could be attributed to the canopy behavior during the wind tunnel experiment. For the CFD simulation, the split portions of the straws were stationary, and straw bending or oscillations were not accounted for. However, during the wind tunnel experiments, continuous oscillation of the plastic straws was observed when the simulated vegetation was subjected to wind, potentially leading to overflows around the vegetation (above and at the sides of the canopy).

Figure 7 shows normalized predicted velocity profiles at various positions within the canopy, as indicated in figure 6.

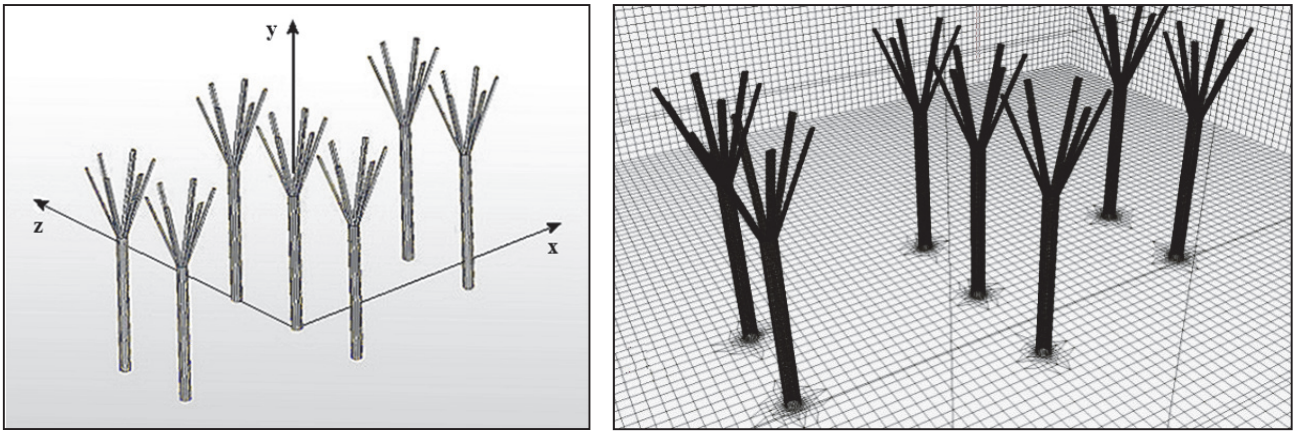


(a) (b)

**Figure 3. (a) Geometry created using Salomé and (b) mesh created using snappyHexMesh for the 100 mm × 200 mm configuration at 220 mm standing vegetation height.**

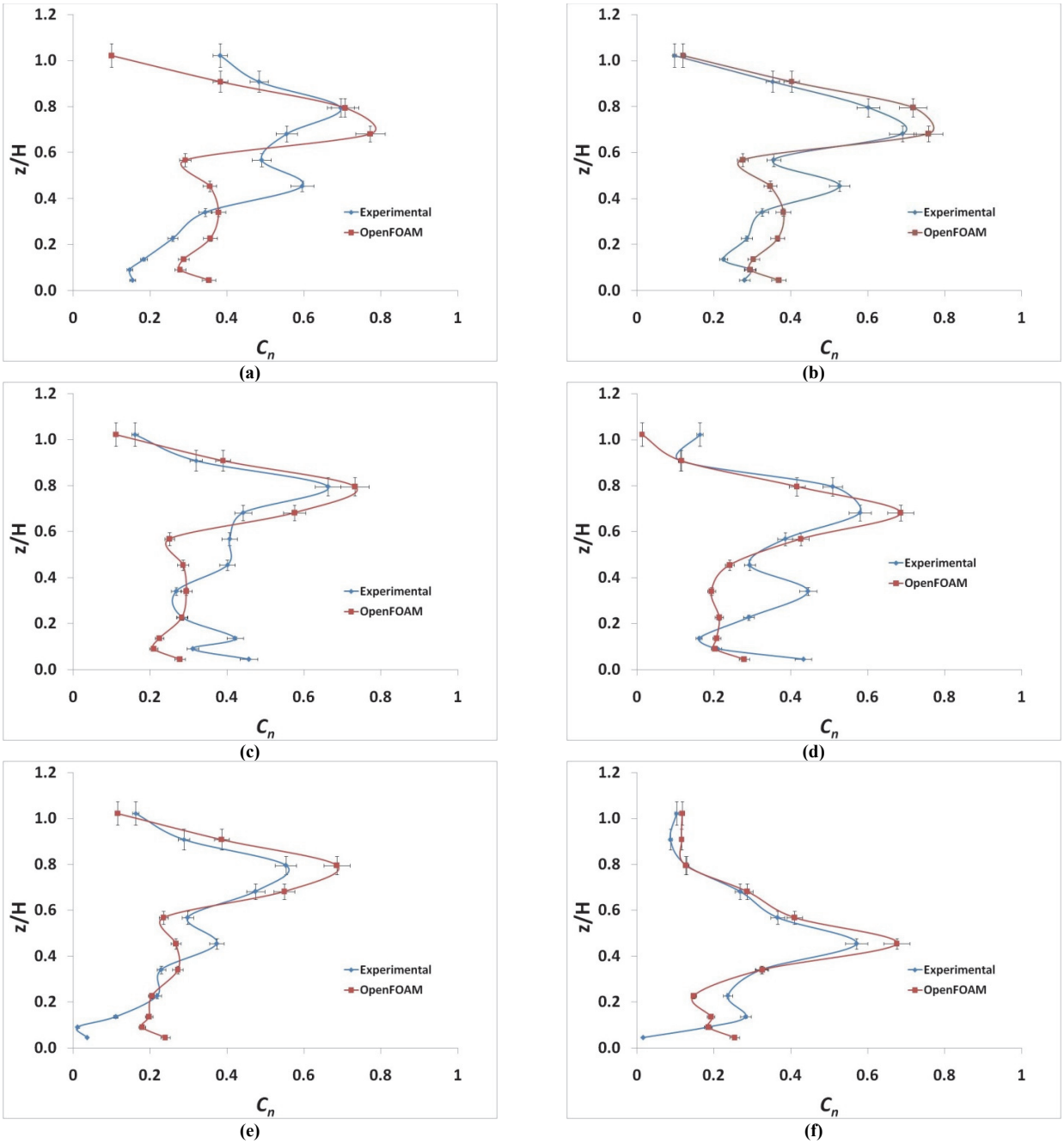


**Figure 4. Vertical profiles of effective drag coefficient ($C_n$) for artificial vegetation spacings of 100 mm × 200 mm at (a) 220 mm and (b) 150 mm heights, 200 mm × 200 mm at (c) 220 mm and (d) 150 mm heights, and 300 mm × 200 mm at (e) 220 mm and (f) 150 mm heights. See figure 6 for an example configuration. Error bars represent values within a 95% confidence interval.**

The same positions were selected for all configurations. Points A to H represent positions between rows (i.e., C, D, F, and G), between canopies within a row (i.e., B, E, and H), and upwind of the vegetation (A). Normalization was achieved by dividing the vertical velocities by the maximum velocity (velocity at the height of the domain, $z$ = 0.9 m, which represents the maximum velocity within the tunnel, measured as free-stream velocity).

The plots in figure 7 show normalized velocity profiles at the wake of the canopy that are identical to observations in previous studies (Cionco and Ellefsen, 1998; Katul et al., 2004; Pyles et al., 2004; Endalew et al., 2009). Positions B and D have identical smooth log profiles for velocity, similar to upwind position A. This is expected because no obstructions were in front of positions A, B, and D, even if they were within the canopy area. Figure 7 also shows that a reduction in wind velocity occurred within the canopy height, and the resistance due to the presence of split straws ($z/H_2$ values of approximately 0.15 to 0.22) caused a drastic decrease in velocity. This is demonstrated by the sharp skew of the profiles toward the left as the wind hit the canopy at positions where standing vegetation obstructed the airflow (i.e., C, E, F, G, and H).

The same behavior of the velocity profiles at the same

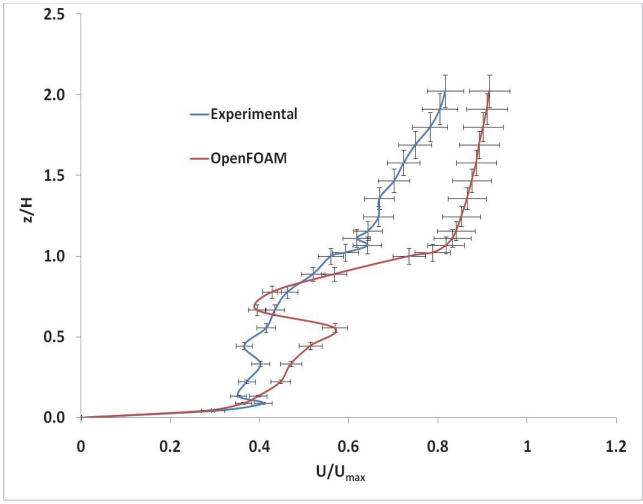


**Figure 5. Comparison of normalized mean velocity profiles from the wind tunnel experiment and CFD simulation based on measurements at the back of canopy for the 100 mm × 200 mm configuration at 220 mm height (*H*), as shown in fig. 6. $U_{max}$ was constant at 15 m s$^{-1}$. Error bars represent values within a 95% confidence interval.**

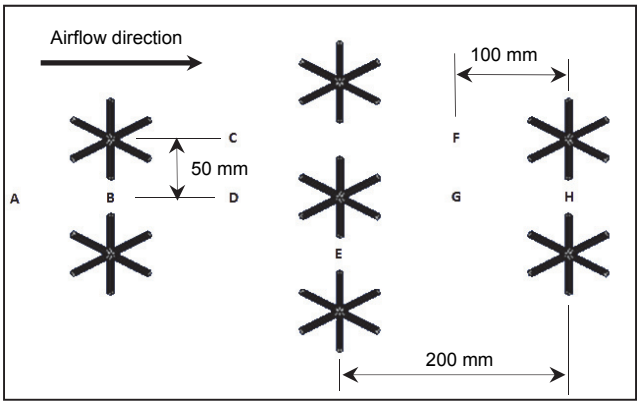


**Figure 6. Top view of the positions considered for velocity profile comparison with the 100 mm × 200 mm configuration. Points A to H are the positions of predicted values corresponding to those in figure 7.**

positions within the canopy was observed with other configurations (fig. 7). The difference between profiles of the same height was that the wake velocities at E and F were slightly lower for denser configurations and lowest for the densest configuration of 100 mm × 200 mm. Obstruction of wind by vegetation is shown by the greater skew toward the left at the region of velocity reduction, implying that the presence of additional standing vegetation led to better sheltering downwind. In addition, comparison of the same density at different heights (150 mm vs. 220 mm) of standing vegetation showed that the area of velocity reduction was greater for taller vegetation.

Investigation of contour plots (fig. 8) of predicted velocities within the standing vegetation shows that a majority of the displaced profiles (above and at the sides of the standing vegetation) were responsible for instantaneous increases in wind velocity, which is because full canopies were present and their resistance was compensated by the presence of overflows and increases in wind velocity around the standing vegetation (Endalew et al., 2009). This region, known as the roughness sublayer (Georgiadis et al., 1996), dictates the turbulence in airflow due to the complexity and three-dimensionality of the canopy structures. A detailed discussion of the regions that comprise the roughness sublayer is given by Endalew et al. (2009). As shown in figure 8, a majority of the velocity reduction occurred in the canopy region where oscillations in airflow occur, rendered by increased entropy of the fluid at the wake and within the canopy.

## CONCLUSIONS

Measured airflow through a simulated canopy was successfully modeled using open-source CFD software (OpenFOAM). Wind speeds measured in a previous wind tunnel experiment compared well to the modeled speeds but differed slightly from the numerical simulation, especially near the crown where split straws were present and where the CFD model underpredicted the measured values. Such discrepancies could be a result of oscillatory motions unaccounted for during the CFD simulation because the geometry was stationary, rather than the dynamic geometry observed during the wind tunnel experiment. Effective drag coefficients computed using wind profiles did not differ significantly ($p < 0.05$) between the experimental and simulated results. Results of this study provide 3-D simulation data of wind flow through a plant canopy. Research into other types of stubble or sparse vegetation during wind events can be similarly conducted on a limited basis using CFD simulation, without the need for labor-intensive wind tunnel studies.

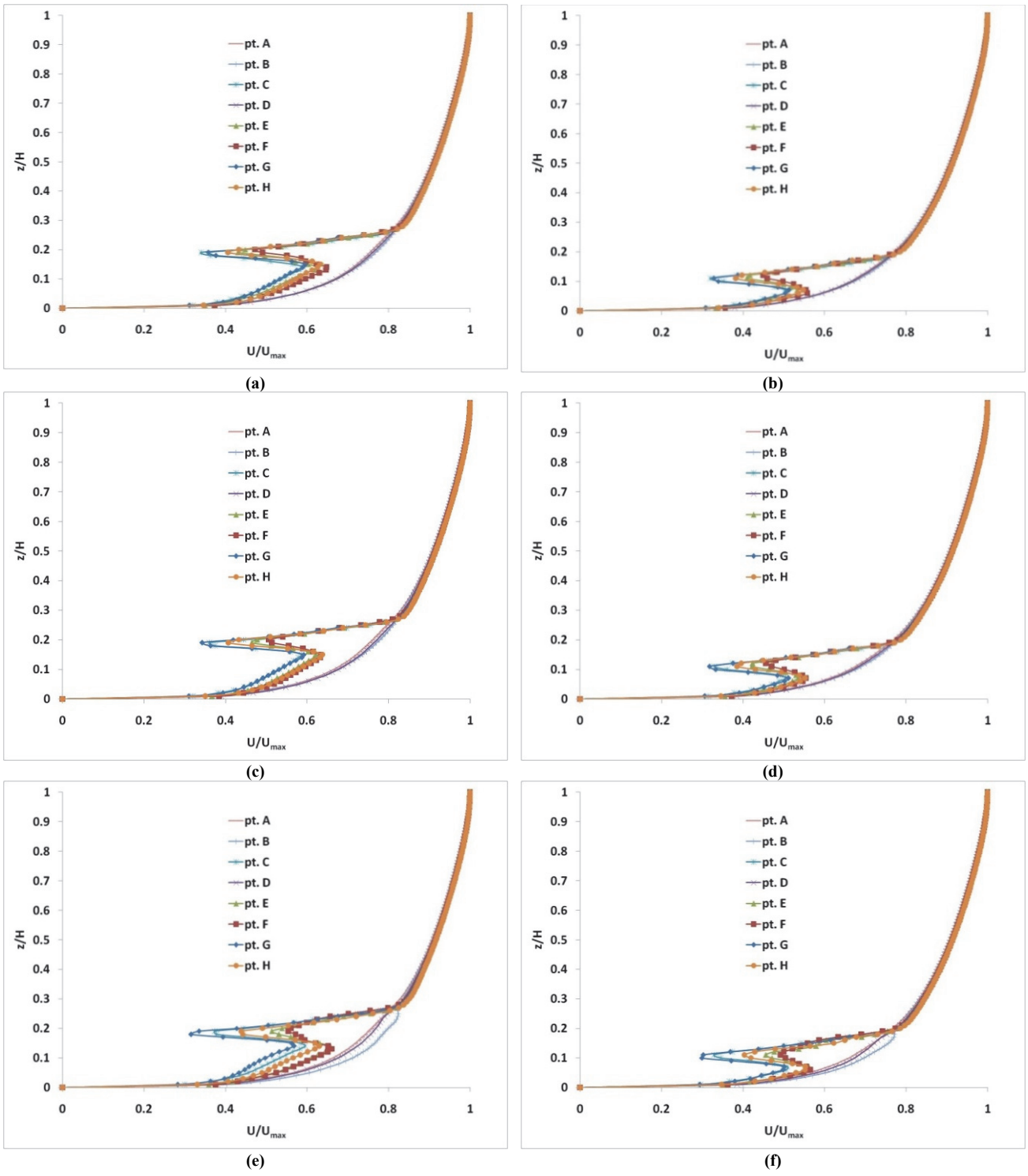


**Figure 7. Comparison of normalized predicted velocity profiles within the canopy for artificial vegetation spacings of 100 mm × 200 mm at (a) 220 mm and (b) 150 mm heights, 200 mm × 200 mm at (c) 220 mm and (d) 150 mm heights, and 300 mm × 200 mm at (e) 220 mm and (f) 150 mm heights. Points A to H represent positions within the canopy, as shown in figure 6.**

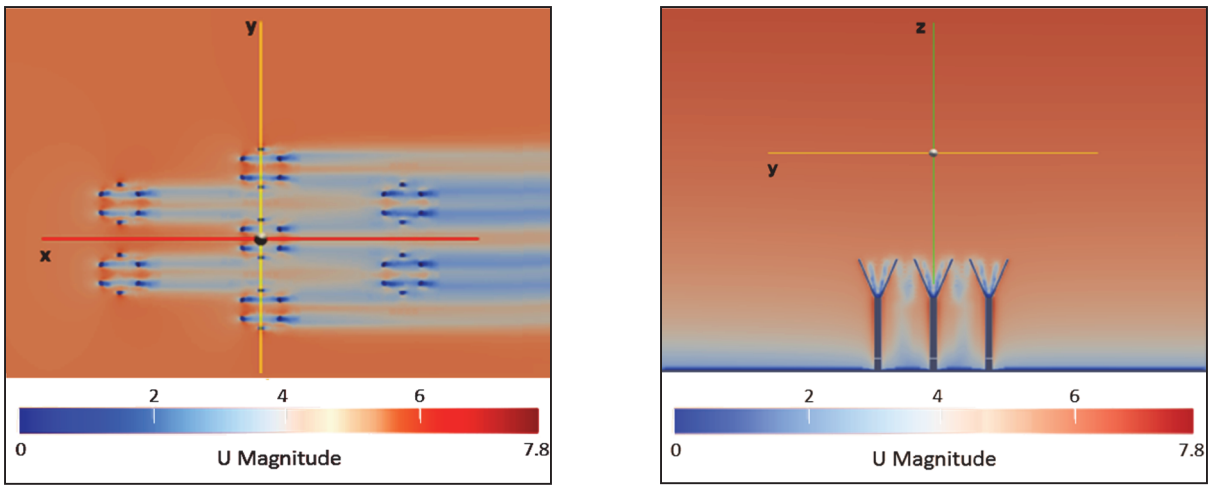


**Figure 8. (a) Top and (b) front views of velocity contours for CFD simulation of artificial standing vegetation.**

## REFERENCES


Bitog, J. P., Lee, I.-B., Hwang, H.-S., Shin, M.-H., Hong, S.-W., Seo, I.-H., ... Pang, Z. (2012). Numerical simulation study of a tree windbreak. *Biosyst. Eng., 111*(1), 40-48. https://doi.org/10.1016/j.biosystemseng.2011.10.006

Bonifacio, H. F., Maghirang, R. G., & Glasgow, L. A. (2014). Numerical simulation of transport of particles emitted from ground-level area source using AERMOD and CFD. *Eng. Appl. Comput. Fluid Mech., 8*(4), 488-502. https://doi.org/10.1080/19942060.2014.11083302

Bourdin, P., & Wilson, J. D. (2008). Windbreak aerodynamics: Is computational fluid dynamics reliable? *Boundary-Layer Meteorol., 126*(2), 181-208. https://doi.org/10.1007/s10546-007-9229-y

Cheng, Y., Lien, F. S., Yee, E., & Sinclair, R. (2003). A comparison of large eddy simulations with a standard *k-* Reynolds-averaged Navier-Stokes model for the prediction of a fully developed turbulent flow over a matrix of cubes. *J. Wind Eng., 91*(11), 1301-1328. https://doi.org/10.1016/j.jweia.2003.08.001

Cionco, R. M., & Ellefsen, R. (1998). High-resolution urban morphology data for urban wind flow modeling. *Atmos. Environ., 32*(1), 7-17. https://doi.org/10.1016/S1352-2310(97)00274-4

Defraeye, T., Blocken, B., Koninckx, E., Hespel, P., & Carmeliet, J. (2010). Aerodynamic study of different cyclist positions: CFD analysis and full-scale wind-tunnel tests. *J. Biomech., 43*(7), 1262-1268. https://doi.org/10.1016/j.jbiomech.2010.01.025

Dong, Z., Gao, S., & Fryrear, D. W. (2001). Drag coefficients, roughness length, and zero-plane displacement height as disturbed by artificial standing vegetation. *J. Arid Environ., 49*(3), 485-505. https://doi.org/10.1006/jare.2001.0807

Endalew, A. M., Hertog, M., Delele, M. A., Baetens, K., Persoons, T., Baelmans, M., ... Verboven, P. (2009). CFD modeling and wind tunnel validation of airflow through plant canopies using 3D canopy architecture. *Intl. J. Heat Fluid Flow, 30*(2), 356-368. https://doi.org/10.1016/j.ijheatfluidflow.2008.12.007

Fryrear, D. W., Stout, J. E., Hagen, L. J., & Vories, E. D. (1991). Wind erosion: Field measurement and analysis. *Trans. ASAE, 34*(1), 155-160. https://doi.org/10.13031/2013.31638

Georgiadis, T., Dalpane, E., Rossi, F., & Nerozzi, F. (1996). Orchard-atmosphere physical exchanges: Modeling the canopy aerodynamics. *Acta Hort., 416*, 177-182. https://doi.org/10.17660/ActaHortic.1996.416.21

Gonzales, H. B., Casada, M. E., Hagen, L. J., Tatarko, J., & Maghirang, R. G. (2017). Sand transport and abrasion within simulated standing vegetation. *Trans. ASABE, 60*(3), 791-802. https://doi.org/10.13031/trans.11878

Gromke, C., Buccolieri, R., Di Sabatino, S., & Ruck, B. (2008). Dispersion study in a street canyon with tree planting by means of wind tunnel and numerical investigations: Evaluation of CFD data with experimental data. *Atmos. Environ., 42*(37), 8640-8650. https://doi.org/10.1016/j.atmosenv.2008.08.019

Guo, L., & Maghirang, R. G. (2012). Numerical simulation of airflow and particle collection by vegetative barriers. *Eng. Appl. Comput. Fluid Mech., 6*(1), 110-122. https://doi.org/10.1080/19942060.2012.11015407

Hagen, L. J. (1996). Crop residue effects on aerodynamic processes and wind erosion. *Theor. Appl. Climatol., 54*(1-2), 39-46. https://doi.org/10.1007/BF00863557

Hagen, L. J., & Armbrust, D. V. (1994). Plant canopy effects on wind erosion saltation. *Trans. ASAE, 37*(2), 461-465. https://doi.org/10.13031/2013.28097

Hagen, L. J., & Casada, M. E. (2013). Effect of canopy leaf distribution on sand transport and abrasion energy. *Aeolian Res., 10*, 37-42. https://doi.org/10.1016/j.aeolia.2013.01.005

He, X., Presley, D. R., Tatarko, J., & Blanco-Canqui, H. (2017). Crop residue harvest impacts wind erodibility and simulated soil loss in the Central Great Plains. *GCB Bioenergy, 10*(3), 213-226. https://doi.org/10.1111/gcbb.12483

Higuera, P., Lara, J. L., & Losada, I. J. (2013). Simulating coastal engineering processes with OpenFOAM. *Coastal Eng., 71*, 119-134. https://doi.org/10.1016/j.coastaleng.2012.06.002

Hyams, D. G. (2013). Curve expert 1.4 software. Retrieved from www.curveexpert.net

Katul, G. G., Mahrt, L., Poggi, D., & Sanz, C. (2004). One- and two-equation models for canopy turbulence. *Boundary-Layer Meteorol., 113*(1), 81-109. https://doi.org/10.1023/B:BOUN.0000037333.48760.e5

Lancaster, N., & Baas, A. (1998). Influence of vegetation cover on sand transport by wind: Field studies at Owens Lake, California. *Earth Surf. Proc. Landforms, 23*(1), 69-82. https://doi.org/10.1002/(sici)1096-9837(199801)23:1<69::aid-esp823>3.0.co;2-g

Lee, I. B., Sase, S., & Sung, S. H. (2007). Evaluation of CFD accuracy for the ventilation study of a naturally ventilated broiler house. *Japan Agric. Res. Qtly., 41*(1), 53-64. https://doi.org/10.6090/jarq.41.53

Lee, S. J., & Lim, H. C. (2001). A numerical study on flow around a triangular prism located behind a porous fence. *Fluid Dyn. Res., 28*(3), 209-221. https://doi.org/10.1016/s0169-5983(00)00030-7

Li, F. R., Kang, L. F., Zhang, H., Zhao, L. Y., Shirato, Y., & Taniyama, I. (2005). Changes in intensity of wind erosion at different stages of degradation development in grasslands of Inner Mongolia, China. *J. Arid Environ., 62*(4), 567-585. https://doi.org/10.1016/j.jaridenv.2005.01.014

Li, W., Wang, F., & Bell, S. (2007). Simulating the sheltering effects of windbreaks in urban outdoor open space. *J. Wind Eng. Ind. Aerodyn., 95*(7), 533-549. https://doi.org/10.1016/j.jweia.2006.11.001

Lin, X. J., Barrington, S., Choiniere, D., & Prasher, S. (2007). Simulation of the effect of windbreaks on odor dispersion. *Biosyst. Eng., 98*(3), 347-363. https://doi.org/10.1016/j.biosystemseng.2007.07.010

Liu, F. (2016). A thorough description of how wall functions are implemented in OpenFOAM. In *Proc. CFD with OpenSource Software* (H. Nilsson, Ed.). Retrieved from http://www.tfd.chalmers.se/~hani/kurser/OS_CFD_2016/FangqingLiu/openfoamFinal.pdf

Lyles, L., & Allison, B. E. (1976). Wind erosion: The protective role of simulated standing stubble. *Trans. ASAE, 19*(1), 61-64. https://doi.org/10.13031/2013.35967

Lysenko, D. A., Ertesvag, I. S., & Rian, K. E. (2013). Modeling of turbulent separated flows using OpenFOAM. *Comput. Fluids, 80*, 408-422. https://doi.org/10.1016/j.compfluid.2012.01.015

Menter, F. R. (1994). Two-equation eddy-viscosity turbulence models for engineering applications. *AIAA J., 32*(8), 1598-1605. https://doi.org/10.2514/3.12149

Musick, H. B., & Gillette, D. A. (1990). Field evaluation of relationships between a vegetation structural parameter and sheltering against wind erosion. *Land Degrad. Devel., 2*(2), 87-94. https://doi.org/10.1002/ldr.3400020203

OpenCFD. (2011). OpenFOAM user guide. Bracknell, UK: OpenCFD. Retrieved from https://www.openfoam.com/documentation/user-guide/

Packwood, A. R. (2000). Flow through porous fences in thick boundary layers: Comparisons between laboratory and numerical experiments. *J. Wind Eng. Ind. Aerodyn., 88*(1), 75-90. https://doi.org/10.1016/S0167-6105(00)00025-8

Patankar, S. V. (1980). *Numerical heat transfer and fluid flow*. Washington, DC: Hemisphere Publishing.

Politis, A. K., Stavropoulos, G. P., Christolis, M. N., Panagopoulos, P. G., Vlachos, N. S., & Markatos, N. C. (2008). Numerical modeling of simulated blood flow in idealized composite arterial coronary grafts: Transient flow. *J. Biomech., 41*(1), 25-39. https://doi.org/10.1016/j.jbiomech.2007.08.007

Pyles, R. D., Paw, U. K., & Falk, M. (2004). Directional wind shear within an old-growth temperate rainforest: Observations and model results. *Agric. Forest Meteorol., 125*(1), 19-31. https://doi.org/10.1016/j.agrformet.2004.03.007

Qiao, A., & Liu, Y. (2008). Medical application oriented blood flow simulation. *Clin. Biomech., 23*(1), S130-S136. https://doi.org/10.1016/j.clinbiomech.2007.09.018

Richards, P. J., & Hoxey, R. P. (1993). Appropriate boundary conditions for computational wind engineering models using the *k*- turbulence model. *J. Wind Eng. Ind. Aerodyn., 46-47*, 145-153. https://doi.org/10.1016/0167-6105(93)90124-7

Rosenfeld, M., Marom, G., & Bitan, A. (2010). Numerical simulation of the airflow across trees in a windbreak. *Boundary-Layer Meteorol., 135*(1), 89-107. https://doi.org/10.1007/s10546-009-9461-8

Santiago, J. L., Martin, F., Cuerva, A., Bezdenejnykh, N., & Sanz-Andres, A. (2007). Experimental and numerical study of wind flow behind windbreaks. *Atmos. Environ., 41*(30), 6406-6420. https://doi.org/10.1016/j.atmosenv.2007.01.014

Stockton, P. H., & Gillette, D. A. (1990). Field measurement of the sheltering effect of vegetation on erodible land surfaces. *Land Degrad. Develop., 2*(2), 77-85. https://doi.org/10.1002/ldr.3400020202

Tiwary, A., Morvan, H. P., & Colls, J. J. (2005). Modeling the size-dependent collection efficiency of hedgerows for ambient aerosols. *J. Aerosol Sci., 37*(8), 990-1015. https://doi.org/10.1016/j.jaerosci.2005.07.004

Toure, A. A., Rajot, J. L., Garba, Z., Marticorena, B., Petit, C., & Sebag, D. (2011). Impact of very low crop residue cover on wind erosion in the Sahel. *Catena, 85*(3), 205-214. https://doi.org/10.1016/j.catena.2011.01.002

Van de Ven, T. A., Fryrear, D. W., & Spaan, W. P. (1989). Vegetation characteristics and soil loss by wind. *J. Soil Water Cons., 44*(4), 347-349.

Wolfe, S. A., & Nickling, W. G. (1993). The protective role of sparse vegetation in wind erosion. *Prog. Phys. Geog., 17*(1), 50-68. https://doi.org/10.1177/030913339301700104

Yeh, C.-P., Tsai, C.-H., & Yang, R.-J. (2010). An investigation into the sheltering performance of porous windbreaks under various wind directions. *J. Wind Eng. Ind. Aerodyn., 98*(10), 520-532. https://doi.org/10.1016/j.jweia.2010.04.002